

## Original Study

## Open Access

Jacek Grosel\*, Wojciech Pakos

# Effect of structure–ground interaction on shrinkage stresses in foundation reinforced concrete elements

<https://doi.org/10.2478/sgem-2025-0013>

received October 11, 2024; accepted April 13, 2025.

**Abstract:** This paper presents a numerical analysis of the shrinkage of reinforced concrete foundations on the ground, known as mat foundations. It presents Finite Element Method (FEM) calculations of a beam and its verification with analytical solutions. Two numerical models of mat foundations have been adopted for the purpose of this study. The first model is a foundation resting directly on the ground, that is, on an elastic Winkler base. The second numerical model consists of layers, that is, a mat foundation and a substructure (lean concrete), taking into account the frictional forces between these layers. The Mohr–Coulomb model was used in the analyses. Conclusions were drawn from the numerical analyses on the influence of the soil substrate on the magnitude of the shrinkage stresses. Modelling the interaction between the foundation and a concrete sole using elastic bonds is clearly suboptimal. Using friction to model this connection is a better approach as it avoids underestimating shrinkage stresses. The differences can be up to an order of magnitude.

**Keywords:** mat foundation; concrete shrinkage; shrinkage of slabs; structure–substructure interaction.

## 1 Introduction

Concrete shrinkage is a phenomenon that almost always occurs and starts when the concrete mix is placed and vibrated. The magnitude and rate of development of shrinkage depend on many factors, among which the

most commonly mentioned in the literature on the subject [1, 2] are relative humidity, type and amount of binder, water content and water to cement ratio, type and content of cement, ratio of fine to coarse aggregate and type of aggregate (its stiffness) and also the size and shape of the element.

A distinction is made between plastic, chemical (autogenous), drying and thermal shrinkage, [1, 3, 4, 5]. Plastic shrinkage refers to the loss of moisture and contraction of the concrete before it sets, while the other types of shrinkage occur as the concrete ages. Drying shrinkage is caused by the loss of water during the drying process. It increases with time and takes place months and years after casting. Chemical shrinkage (often called autogenous shrinkage) occurs rapidly in the days or weeks after casting. It results from chemical reactions taking place in the concrete mix. Thermal shrinkage is a change in the dimensions of a component due to a reduction in the temperature of the concrete as the heat of hydration is dissipated. This shrinkage occurs during the first few hours (or days) after setting.

In the absence of restrained boundaries (i.e. connections to other structural elements) and internal reinforcing bars, shrinkage will reduce the dimensions of the elements creating stresses that would give a zero resultant. Therefore, there are no stresses other than the self-balancing stresses resulting from the difference in the rate of heat or moisture transfer between the surface and the interior of the concrete element. In the context of reinforced concrete, the scenario considered is purely hypothetical, given the presence of internal ties and the fact that the majority of structural elements are subject to restrained boundaries. The effect of the presence of internal bonds against shrinkage is described, among others, in references [3] and [6].

The potential for significant shrinkage deformations is of concern because of their ability to induce significant cracking. This, in turn, can lead to corrosion of the steel and reduction in the load-carrying capacity of the structure. To mitigate the problem of shrinkage, a specific

\*Corresponding author: Jacek Grosel, Wrocław University of Science and Technology, Faculty of Civil Engineering, pl. Grunwaldzki 11, 50-370 Wrocław, Poland, E-mail: jacek.grosel@pwr.edu.pl

Wojciech Pakos, Wrocław University of Science and Technology, Faculty of Civil Engineering, pl. Grunwaldzki 11, 50-370 Wrocław, Poland

type of cement is used in conjunction with concrete additives and admixtures. In addition to the above, it is imperative that great care is taken during curing of the concrete and reinforcement to limit the development of shrinkage cracks.

The issue of shrinkage analysis in reinforced concrete structures, particularly in the context of bridges, has been the subject of extensive research over a long period of time. Numerical approaches [7] and analytical solutions have been established, particularly for deep bridge beams (2 m or more in height) [8]. In contrast to foundations (continuous strip footings or mat foundations), there is an absence of interaction between the structure and the ground for beams (such as bridges or floors). In the case of ground-based structures, soil parameters are not generally considered [7] or are only taken into account due to the limitations of water contained in the concrete mixture [9]. Consequently, it is still common in practice to encounter numerous cases of unforeseen cracking of reinforced concrete structures, especially mat foundation, where there is an interaction between the structure and the soil.

In this paper, a numerical analysis of the shrinkage of mat foundations was carried out. The influence of concrete shrinkage on the stresses in the mat foundation was investigated. Concrete shrinkage associated with concrete drying out (the so-called first critical term [10]) was modelled with Finite Element Method (FEM) calculation with a uniform temperature gradient. The foundation was modelled as an elastic Winkler foundation with stiffness parameters  $k_x$ ,  $k_y$ ,  $k_z$ . The effect of different values of the stiffness coefficients  $k$  was considered. The numerical analyses also considered the case of friction between the mat foundation and the substructure (lean concrete substructure). The numerical analyses also considered the case of friction between the mat foundation and the supporting substructure.

## 2 Verification of FEM calculations

The purpose of this section is to verify the FEM calculations. For the purpose of this verification, the standard structural case was not analysed, but the data has been taken arbitrarily. For the calculations, the material parameters were taken as in the second numerical example (section 3), where justification of the taken values is given and the necessary calculations are included. Shrinkage in the FEM model was simulated by changing (lowering) the temperature, resulting in a reduction in the dimensions

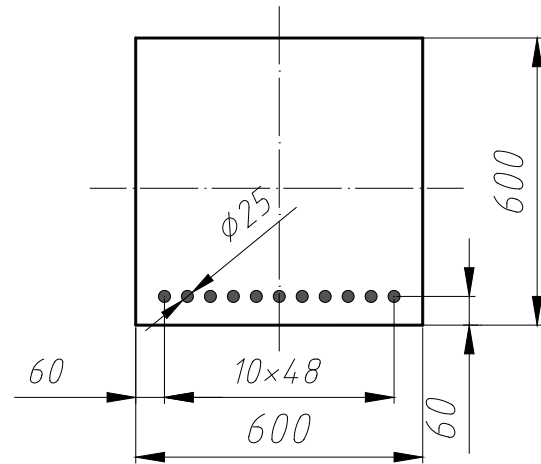


**Figure 1:** Cross section of reinforced concrete beam with reinforcing bar arrangement, dimensions in millimetres.

of the concrete elements corresponding to the shrinkage. The elements modelling the reinforcement have no thermal deformation. Calculations for the same data were performed using the analytical formulae derived below. The results obtained from FEM were compared to those obtained from the analytical solutions.

### 2.1 The geometry and material parameters

This paper considers a  $0.6 \times 0.6 \times 10$  m, reinforced concrete beam with the following material parameters.

Concrete:

- Young's modulus  $E_{cm} = 30.8$  GPa,
- Poisson's ratio  $\nu = 0.2$ ,
- coefficient of thermal expansion  $\alpha_t = 10^{-5}$   $1/^\circ\text{C}$  and
- density  $\rho = 2400$   $\text{kg/m}^3$ .
- uniform temperature gradient:  $\Delta T = 24.6$   $^\circ\text{C}$

Reinforcement:

- elasticity modulus  $E_s = 200$  GPa,
- Poisson's ratio  $\nu = 0.3$  and
- density  $\rho = 7850$   $\text{kg/m}^3$ .

A reinforcement ratio of 1.5% ( $0.015 \times 60 \times 60 = 54.0$   $\text{cm}^2$ ) was assumed for the calculations, so 11 bars of  $\phi 25$  with a reinforcement cross-sectional area of  $54.0$   $\text{cm}^2$  were assumed. The cross section of the beam with the location of the reinforcing bars is shown in Figure 1.

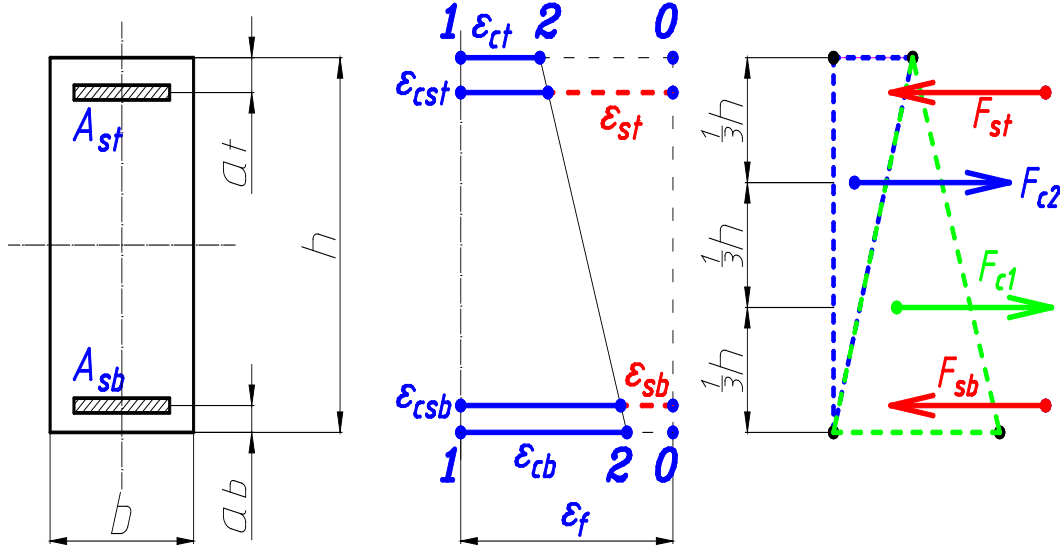


Figure 2: The section under analysis, deformations of cross section, forces due to strain.

## 2.2 Analytical approach

A rectangular section of concrete (with Young’s modulus  $E_c$ ) is considered, with reinforcing steel (with Young’s modulus  $E_s$ ) added in upper and lower levels. The top reinforcement has a section  $A_{st}$ , with its centre of gravity located at a distance  $a_t$  from the top edge. The bottom reinforcement has a section  $A_{sb}$ , with its centre of gravity located at a distance  $a_b$  from the bottom edge.

The section under analysis and its deformations are displayed in Figure 2. The following designations have been adopted for the purpose of clarification:

- line ‘0-0’ represents the initial state,
- line ‘1-1’ represents the state of the section after free shrinkage, that is, shrinkage without external or internal constraints and
- line ‘2-2’ represents the final state, after constrained shrinkage, that is, limited by internal ties such as reinforcement.

The assumption is made that plane sections remain plane, as in the paper [11], and the following designations are introduced:

- $\epsilon_f$  – free strain
- $\epsilon_{cb}$  – strain of concrete at the lower edge of the section
- $\epsilon_{ct}$  – strain of concrete at the upper edge of the section
- $\epsilon_{csb}$  – strain of concrete at the lower reinforcement level
- $\epsilon_{cst}$  – strain of concrete at the upper reinforcement level

- $\epsilon_{sb}$  – strain of steel at the level of the lower reinforcement (contraction)
- $\epsilon_{st}$  – strain of steel at the level of the upper reinforcement (contraction)
- $A_c = b \times h$  – concrete cross-sectional area
- $A_{sb} = \mu_b \times A_c$  – area of the lower reinforcement
- $A_{st} = \mu_t \times A_c$  – area of the bottom reinforcement
- $a_t, a_b$  – top/bottom concrete cover
- $n_0 = E_s/E_c$  – relative stiffness, that is, ratio of Young’s modulus of steel to concrete
- $F_{sb}, F_{st}$  – force in the upper and the lower reinforcement, respectively
- $F_{c1}, F_{c2}$  – part of the force in concrete (the total force in the concrete is split into two components)

In accordance with the aforementioned assumptions, it is possible to derive two equilibrium equations. The first of these is for the equilibrium of forces along the axis of the bar (axial force equilibrium), and the second is for the equilibrium of moments. When these equations are considered in conjunction with the assumption of planar sections, they take the following forms.

$$\begin{cases} \sum X = 0: & F_{c1} + F_{c2} - F_{sb} - F_{st} = 0 \\ \sum M_1 = 0: & F_{c1} \cdot \frac{1}{3}h + F_{c2} \cdot \frac{2}{3}h - F_{sb} \cdot a_b - F_{st} \cdot (h - a_t) = 0 \end{cases} \quad (1)$$

$$\begin{aligned} \sum X = 0: \\ \frac{1}{2} E_c b h \epsilon_{cb} + \frac{1}{2} E_c b h \epsilon_{ct} - E_c b h n_0 \left[ -\frac{(-a_b+h)(\epsilon_{cb}-\epsilon_{ct})}{h} - \epsilon_{ct} + \epsilon_f \right] \mu_b + (2) \\ + E_c b h n_0 \left[ -\frac{a_t(\epsilon_{cb}-\epsilon_{ct})}{h} - \epsilon_{ct} + \epsilon_f \right] \mu_t = 0 \end{aligned}$$

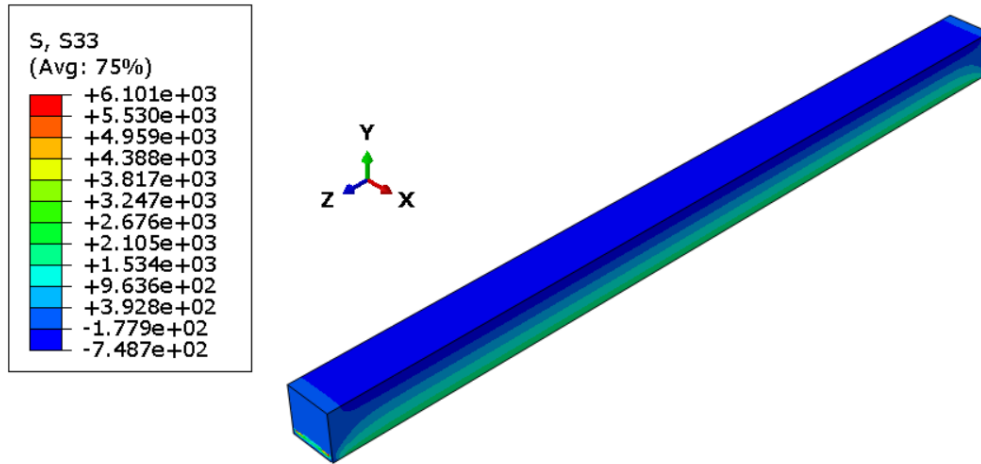


Figure 3: Stress  $S_{33} = S_{zz}$  (kPa) in the concrete beam.

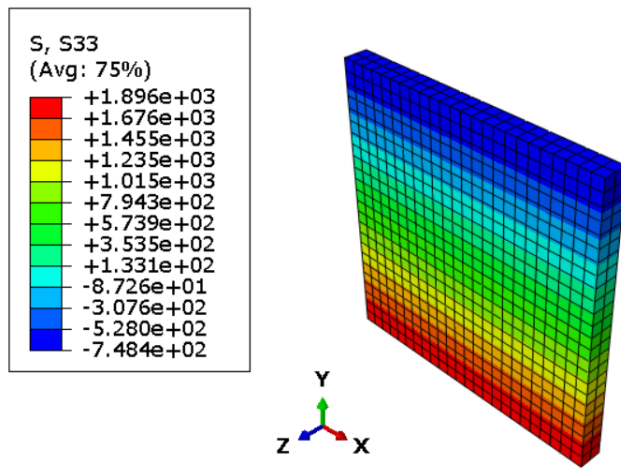


Figure 4: Stresses  $S_{33} = S_{zz}$  (kPa) in the cross section at the mid-span of a concrete beam.

$$\Sigma M_1 = 0:$$

$$\frac{1}{6} E_c b h^2 \varepsilon_{cb} + \frac{1}{3} E_c b h^2 \varepsilon_{ct} +$$

$$- E_c a_b b h n_0 \left[ -\frac{(-a_b+h)(\varepsilon_{cb}-\varepsilon_{ct})}{h} - \varepsilon_{ct} + \varepsilon_f \right] \mu_b + \quad (3)$$

$$- E_c b h (h - a_t) n_0 \left[ -\frac{a_t(\varepsilon_{cb}-\varepsilon_{ct})}{h} - \varepsilon_{ct} + \varepsilon_f \right] \mu_t = 0$$

The system under consideration comprises two equations with two unknowns. The solutions to these equations are as follows:

$$\varepsilon_{ct} = \frac{2n_0\varepsilon_f[(3a_b-h)h\mu_b + (h(-3a_t+2h)+6(a_t+a_b-h)^2n_0\mu_b)\mu_t]}{12a_b^2n_0\mu_b + h[h+4(-3a_b+h)n_0\mu_b] + 4n_0[3a_t^2-3a_t h+h^2+3(a_b+a_t-h)^2n_0\mu_b] \mu_t} \quad (4)$$

$$\varepsilon_{cb} = \frac{2n_0\varepsilon_f[(-3a_b+2h)h\mu_b + (h(3a_t-h)+6(a_t+a_b-h)^2n_0\mu_b)\mu_t]}{12a_b^2n_0\mu_b + h[h+4(-3a_b+h)n_0\mu_b] + 4n_0[3a_t^2-3a_t h+h^2+3(a_b+a_t-h)^2n_0\mu_b] \mu_t} \quad (5)$$

If the section is reinforced only at the bottom, the results simplify to the form:

$$\varepsilon_{ct} = \frac{2(3a_b-h)h n_0 \varepsilon_f \mu_b}{h^2 + 4(3a_b^2 - 3a_b h + h^2) n_0 \mu_b} \quad (6)$$

$$\varepsilon_{cb} = \frac{2(-3a_b+2h)h n_0 \varepsilon_f \mu_b}{h^2 + 4(3a_b^2 - 3a_b h + h^2) n_0 \mu_b} \quad (7)$$

Using the data indicated in section 2.1, the following results are obtained:

$$\varepsilon_{cb} = 6.34 \times 10^{-5} \quad (8)$$

$$\varepsilon_{ct} = -2.61 \times 10^{-5} \quad (9)$$

$$\varepsilon_{sb} = 1.92 \times 10^{-4} \quad (10)$$

which gives stresses

$$\sigma_{cb} = 1.95 \text{ MPa} \quad (11)$$

$$\sigma_{ct} = -0.80 \text{ MPa} \quad (12)$$

$$\sigma_{sb} = 38.30 \text{ MPa} \quad (13)$$

## 2.3 A numerical approach

The numerical model of a reinforced concrete beam was created using Abaqus FEM software [12] (Fig. 3). The concrete beam is represented by general purpose

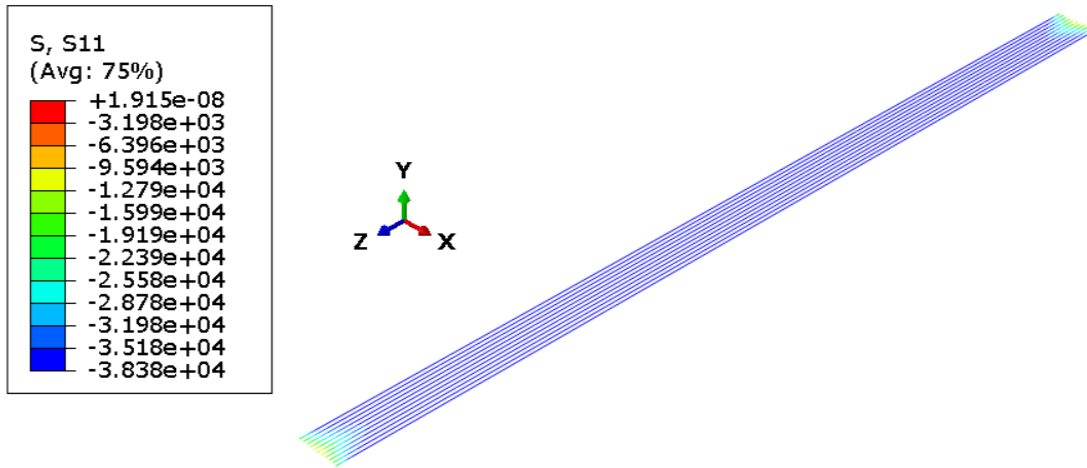


Figure 5: Stress  $S_{11} = S_{zz}$  (kPa) in the reinforcement.

Table 1: Results from analytical and numerical FEM solution.

	Stresses (MPa)			Remarks
	Analytical solution $\sigma_A$	Numerical solution (FEM) $\sigma_F$	Relative error $\Delta\sigma$ (%)	
Concrete, the lower edge of the section	1.95	1.896	2.8%	Tension
Concrete, the upper edge of the section	-0.80	-0.748	6.5%	Compression
Reinforcing steel bars	-38.30	-38.38	0.2%	Compression

eight-node linear hexahedral elements of type C3D8 and reinforcement by truss elements. The numerical model assumed a Winkler substrate with a very low value of stiffness ( $k_x = k_y = k_z = 1 \cdot 10^{-5} \text{ kN/m}^3$ ) to obtain the effect of an unsupported beam (i.e. beam without substrate), to be in accordance with the analytical calculations.

The numerical calculations yielded stresses at the centre of the beam span of 1.896 MPa (tensile stresses, Fig. 4) at the bottom of the beam cross section and -0.748 MPa (compressive stresses, Fig. 4) at the top. In comparison, the stresses in the reinforcing bars were found to be -38.38 MPa (compressive stresses, Fig. 5).

### 2.4 Discussion of numerical results

A comparison of the results obtained from analytical and numerical (FEM) calculations is provided in Table 1. The stress values obtained from the numerical calculations demonstrate a high degree of agreement with the stress values obtained from the analytical solutions. The differences in the values obtained may be attributed to the FEM numerical modelling. The FEM model assumed a Winkler substrate with very low stiffness, while the analytical solution refers to a completely unsupported

beam. The relative error was calculated using the formula  $\Delta\sigma = (\sigma_F - \sigma_A) / \sigma_A (\%)$ .

## 3 Calculation example – a mat foundation

This section presents a numerical example of a mat foundation, taking into account the foundation–soil interaction. The soil was modelled as either a Winkler foundation (model ‘A’) or as a combination of elastic bonds in the vertical direction and frictional forces in the horizontal direction (model ‘B’). Both models are schematically shown in Figure 6. Although more sophisticated ground models have been developed, due to good approximations and its simplicity, the Winkler model is widely used in engineering practice [13]. The objective of the numerical analyses presented here is to ascertain whether there is a significant difference in performance between these ground models (models ‘A’ and ‘B’). Movements of the foundation sole associated with shrinkage deformation in the case of model ‘A’ always occur and are inversely proportional to the horizontal stiffness of the subsoil. In the case of model

'B', movement will occur if the forces due to shrinkage exceed a certain limit depending on the frictional forces. The hypothesis is that model 'B' may yield higher stress values, as in this model, the movement of the foundation sole may not occur, which is equivalent to external ties. At the same time, the foundation-sole interaction in model 'B' is closer to reality. In the presented examples, the mat foundation is loaded only with its own weight, corresponding to a situation where the building structure has not yet been built on the foundation mat. This is an early stage of construction, and therefore, the effect of autogenous shrinkage is analysed. In the case of completed construction, the load on the mat is increased, causing an increase in frictional forces. This design situation occurs a long time after the foundation mat has been constructed, and in this case, shrinkage from drying out will be predominant. This case is not analysed in this article but will be the subject of subsequent publications.

### 3.1 The geometry and material properties

This paper considers a  $45 \times 30$  m, 60-cm-thick concrete mat foundation with the following material parameters [10, 14]:

- concrete with strength class C35/45,  $f_{cm} = 43$  MPa,  $f_{ck} = 35$  MPa [15] made of Portland cement CEM I, class CR;
- elasticity modulus  $E_{cm} = k_E \cdot f_{cm}^{1/3}$ , for concrete with quartzite aggregates  $k_E = 9500$ ,  $E_{cm} = 33.3$  GPa;
- modulus of elasticity for concrete younger than 28 days is given by formula (B.4) from [15]  $E_{cm}(t) = E_{cm} \cdot \beta_{cc}^{1/3}(t)$  and  $\beta_{cc}$  is given by formula (B.2) from [15]

$$\beta_{cc}(t) = \exp \left[ s_c \left( 1 - \sqrt{\frac{t_{ref}}{t}} \right) \sqrt{\frac{28}{t_{ref}}} \right],$$

$s_c = 0.3$  for class CR and  $f_{ck} \leq 35$  MPa

for 7-day concrete  $E_{cm}(7) = E_{cm} \cdot \beta_{cc}^{1/3}(7) = 0.926 E_{cm} = 30.8$  GPa;

- Poisson's ratio  $\nu = 0.2$ ;
- coefficient of thermal expansion  $\alpha_t = 10^{-5} 1/^\circ\text{C}$  and
- density  $\rho = 2400$  kg/m<sup>3</sup>.

Calculation of hardening temperature of concrete in adiabatic conditions (i.e. no heat exchange with the environment)

$$\Delta T_{adiab} = \frac{C \cdot Q_7}{c_b \cdot \rho_b} \quad (14)$$

where:  $C$  – amount of cement in 1 m<sup>3</sup> of concrete (kg),  $C = 300$  kg,  $c_b$  – specific heat of concrete, [kJ/(kg °C)],  $c_b = 1$  kJ/kg °C,  $\rho_b$  – volumetric mass density of concrete (kg/m<sup>3</sup>),

$\rho_b = 2400$  kg/m<sup>3</sup>,  $Q_7$  – hydration heat of cement after 7 days of hardening (kJ/kg),  $Q_7 = 325$  kJ/kg,

$$\Delta T_{adiab} = \frac{300 \cdot 325}{1 \cdot 2400} = 40.6^\circ\text{C} \quad (15)$$

The corrected (reduced) hardening temperature, calculated using a reduction factor that takes into account heat exchange with the environment and non-adiabatic conditions inside the element, is  $\chi = 0.65$  for foundation mats with a thickness of less than 1 m [14].

$$\Delta T_{adiab}^{red} = \chi \cdot \Delta T_{adiab} = 0.65 \cdot 40.6 = 26.4^\circ\text{C} \quad (16)$$

The initial temperature of the concrete mix ( $T_{c0}$ ) was assumed to be 20°C, the same as the ambient temperature ( $T_a$ ),

$$T_{c0} = T_a = 20.0^\circ\text{C} \quad (17)$$

Calculation of temperature inside the element  $T_{in}$ :

$$T_{in} = T_{c0} + \Delta T_{adiab}^{red} = 46.4^\circ\text{C} \quad (18)$$

and the temperature on the surface of the element:

$$T_p = T_{in} + \frac{T_a - T_{in}}{\frac{1}{2}h + 2\frac{\lambda_c}{\alpha_c}} \cdot \frac{h}{2} \quad (19)$$

where:  $h$  – thickness of the element (m),  $\lambda_c$  – value of thermal conductivity coefficient of concrete (W/(m °C)), for quartzite aggregate is equal to [14]:

$$\lambda_b = 3.4 \text{ W/(m} \cdot ^\circ\text{C)} \quad (20)$$

$\alpha_c$  – coefficient of heat exchange on the surface of a concrete member [W/(m<sup>2</sup> °C)], coefficient depending on the speed of air movement around the concrete element, for air velocity equals to zero [14]:

$$\alpha_c = 6.0 \text{ W/(m}^2 \cdot ^\circ\text{C)} \quad (21)$$

$$T_p = 46.4 + \frac{20 - 46.4}{\frac{1}{2} \cdot 0.6 + 2 \cdot \frac{3.4}{6.0}} \cdot \frac{0.6}{2} = 40.9^\circ\text{C} \quad (22)$$

mean temperature at the thickness of the foundation:

$$T_m = T_{in} - \frac{1}{3}(T_{in} - T_p) = 46.4 - \frac{1}{3}(46.4 - 40.9) = 44.6^\circ\text{C} \quad (23)$$

temperature difference causing deformation

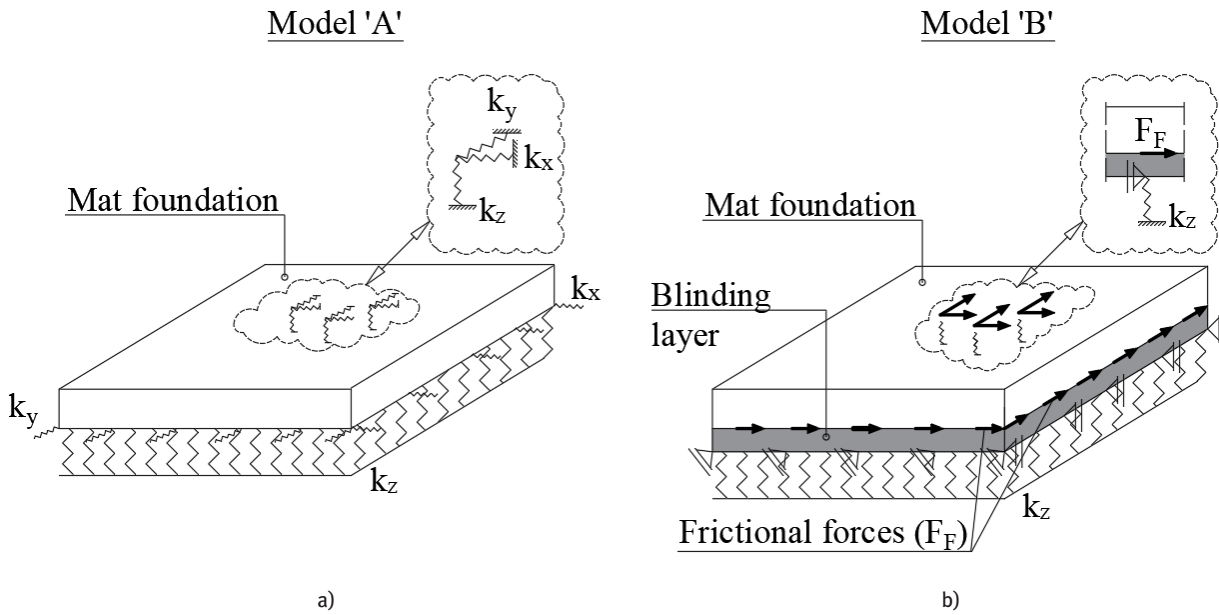


Figure 6: Structure model diagrams adopted for numerical analyses.

$$\Delta T = T_m - T_a = 24.6 \text{ } ^\circ\text{C} \quad (24)$$

In this paper, two numerical models of the mat foundation were adopted for the analyses. The first model (cf. Fig. 6a) is a mat foundation that rests directly on a Winkler elastic foundation with vertical elastic coefficients  $k_z$  and horizontal elastic coefficients  $k_x$  and  $k_y$ . The horizontal elasticity coefficients were taken as follows

$$k_x = k_y = \mu k_z \quad (25)$$

in which  $\mu$  is the coefficient of friction between the soil and the foundation. It was further assumed that the slab lies on a sliding layer, that is, the coefficient of friction between the two layers of special foil is  $\mu = 0.08$ . Special foil covers or sheets with a very low coefficient of friction (0.05 up to 0.10) are used in the construction of foundation supports [16]. For the numerical calculations, the following assumptions were made:  $k_z = 50,000 \text{ kN/m}^3$  and  $k_x = k_y = 0.08k_z = 4000 \text{ kN/m}^3$ .

The numerical model shown in Fig. 6b consists of two slabs: a mat foundation and a blinding layer (lean concrete substructure). The slab modelling the substructure was supported in the vertical direction by elastic bonds (three different values of stiffness were considered for these bonds) and in the horizontal direction by bonds of infinite stiffness. The modelling of friction between the concrete slabs was conducted through the utilisation of the classical isotropic Coulomb friction model in Abaqus,

assuming contact between two slab surfaces. Two friction coefficients,  $\mu = 0.1$  and  $\mu = 0.5$ , were considered in the calculations. Firstly, a low coefficient of friction was adopted to facilitate a comparison of the results obtained from this 'B' model with those obtained from the Winkler substrate-based plate model (model 'A'). Subsequently, a second, five-fold higher friction coefficient was implemented to investigate the effect of friction variation on stresses. Finally, three values of stiffness coefficient  $k_z$  were included in the analysis, with these values covering the range of stiffness coefficients found in construction – compare Table 2.

- For weak soils:  $k_z = 10,000 \text{ kN/m}^3$
- For medium soils:  $k_z = 50,000 \text{ kN/m}^3$
- For strong soils:  $k_z = 100,000 \text{ kN/m}^3$

The bearing capacity condition Mohr–Coulomb for non-cohesive soils is described by the formula:

$$\tau > \sigma \tan (\varphi) \quad (26)$$

When the shear stresses ( $\tau$ ) are greater than the normal stress ( $\sigma$ ) multiplied by the tangent of the internal friction angle ( $\tan \varphi$ ), plasticisation occurs and adjacent layers move relative to each other. An analogous situation occurs when two layers are considered to be bonded by friction. If the force opposing the friction is greater, slippage will occur. The frictional force is proportional to the pressure, therefore the following analogies are legitimate: normal

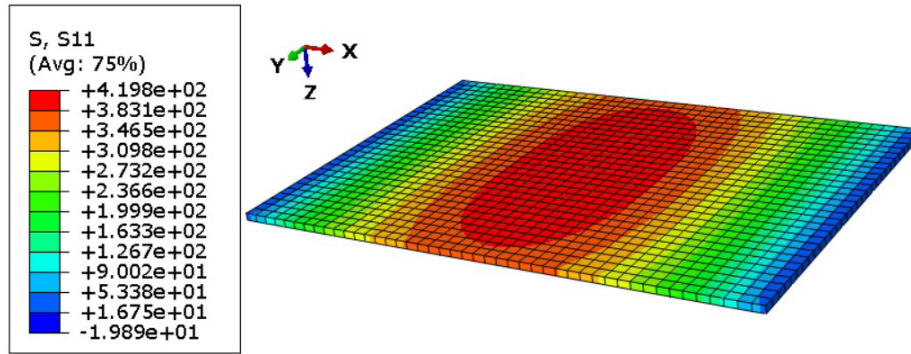


Figure 7: Stress  $S_{11} = \sigma_x$  (kPa) in the concrete slab founded on soil (Winkler model:  $k_z = 50,000 \text{ kN/m}^3$ ,  $k_x = k_y = 4000 \text{ kN/m}^3$ ).

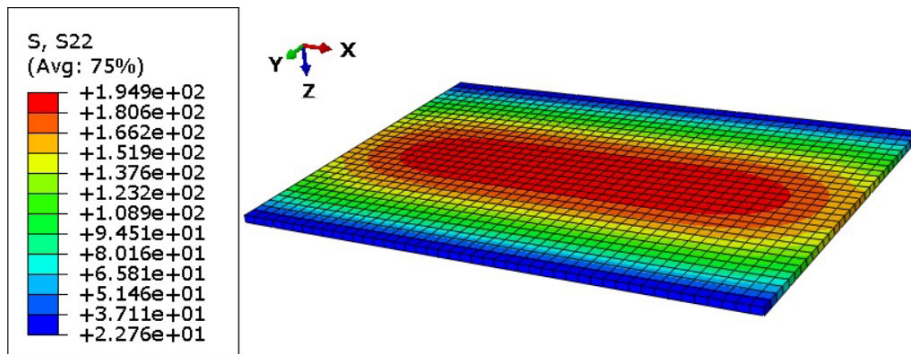


Figure 8: Stress  $S_{22} = \sigma_y$  (kPa) in the concrete slab founded on soil (Winkler model:  $k_z = 50,000 \text{ kN/m}^3$ ,  $k_x = k_y = 4000 \text{ kN/m}^3$ ).

Table 2 Range of modulus of subgrade reaction  $k_z$  based on [13].:

Soil	$k_z$ (kN/m <sup>3</sup> )
Loose sand	4800–16,000
Medium dense sand	9600–80,000
Dense sand	64,000–128,000
Clayey medium dense sand	32,000–80,000
Silty medium dense sand	24,000–48,000
Clayey soil:	
$q_a < 200 \text{ kPa}$	12,000–24,000
$200 < q_a < 800 \text{ kPa}$	24,000–48,000
$q_a > 800 \text{ kPa}$	>48,000

where  $q_a$  is bearing capacity furnished in kPa.

force  $\sim \sigma \tan(\varphi)$ , friction force  $\sim \tau$ . Given the above, the use of frictional bonds for modelling ground with Mohr–Coulomb condition is legitimate.

The load on the mat foundation is a uniform temperature gradient:  $\Delta T = 24.6^\circ\text{C}$  – this value was derived above. In both models ('A' and 'B'), the load was dead

weight. The calculations were carried out using FEM in Abaqus. The mat foundation and the substructure slab (lean concrete base) were modelled using solid elements.

### 3.2 Numerical results

This section presents the results of the numerical calculations. The figures show and the tables summarise the normal stresses  $S_{11} = \sigma_x$  and  $S_{22} = \sigma_y$ , such that the  $\sigma_x$  stresses act in the direction of the long side of the mat foundation and the  $\sigma_y$  stresses act in the direction of the short side. The results obtained for model 'A' (mat foundation resting on Winkler elastic base) are shown in Figures 7 and 8. The results of the calculations for model 'A' are presented in Table 2 under the assumption of a friction coefficient of 0.1. This is undertaken for the purpose of facilitating a comparison with the results obtained from the calculations for model 'B'.

Figures 9–12 show the stresses  $S_{11} = \sigma_x$  and  $S_{22} = \sigma_y$  obtained from the numerical calculations for model 'B' (mat foundation resting on a lean concrete sublayer) with different values of the friction coefficient and different

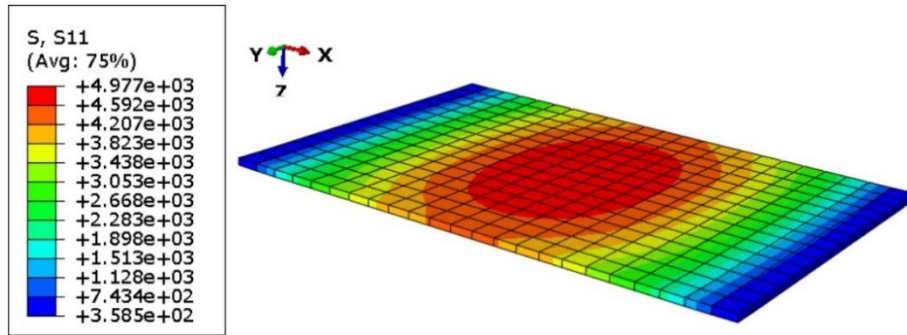


Figure 9: Stress  $S_{11} = \sigma_x$  (kPa) in the concrete slab resting on the lean concrete substructure: friction coefficient  $\mu = 0.1$ ,  $k_z = 50,000$  kN/m<sup>3</sup>.

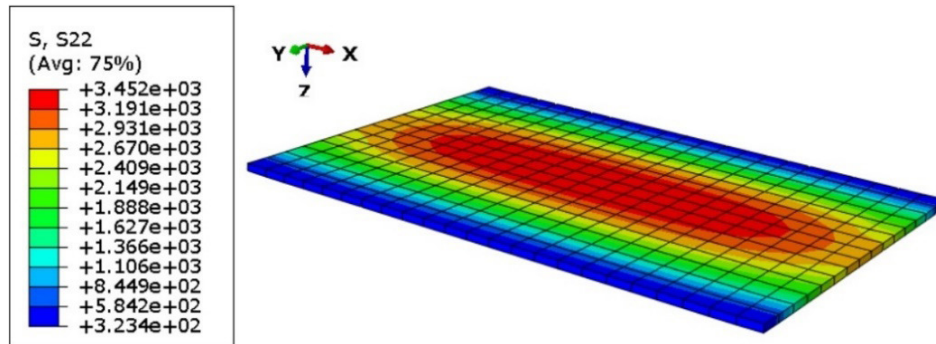


Figure 10: Stress  $S_{22} = \sigma_y$  (kPa) in the concrete slab resting on the lean concrete substructure: friction coefficient  $\mu = 0.1$ ,  $k_z = 50,000$  kN/m<sup>3</sup>.

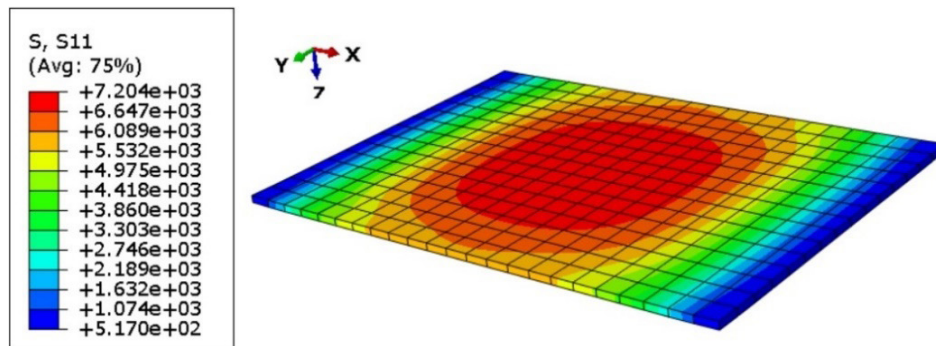


Figure 11: Stress  $S_{11} = \sigma_x$  (kPa) in the concrete slab resting on the lean concrete substructure: friction coefficient  $\mu = 0.5$ ,  $k_z = 10,000$  kN/m<sup>3</sup>.

values of the stiffness coefficient  $k_z$  of the soil substrate. Table 2 summarises the results of the maximum stresses  $\sigma_x$  and  $\sigma_y$ .

### 3.3 Discussion of numerical results

The results obtained in model ‘A’ (slab on Winkler substrate) are similar (qualitatively and quantitatively) to the results of the numerical calculations presented in [10]. In this model, the maximum tensile stress  $S_{11} = \sigma_x$

is 0.42 MPa, while the authors of the book [10] gave the maximum tensile stress value of 0.47 MPa.

A comparison of models ‘A’ and ‘B’, that is, an analysis of the second and third first rows of Table 3, reveals a substantial discrepancy in the results obtained by these models. Specifically, model ‘B’ yields results that are 11 times higher for  $\sigma_x$  stresses and 15 times higher for  $\sigma_y$  stresses. These discrepancies are greater than one order of magnitude, thereby signifying the Winkler model’s inadequacy in considering the shrinkage of concrete elements in conjunction with the simultaneous action of

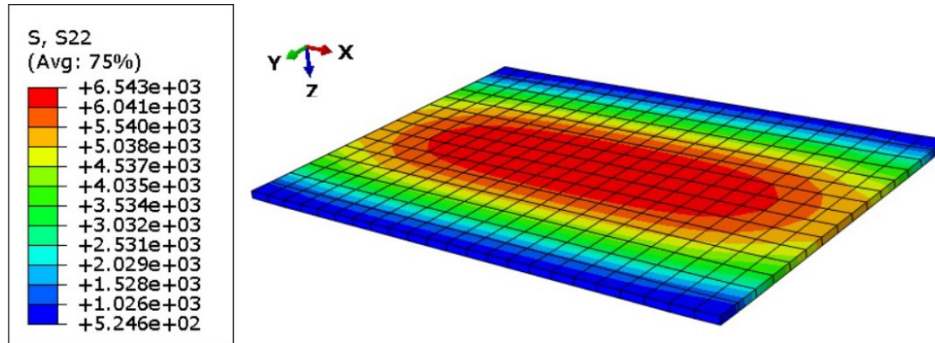


Figure 12: Stress  $S_{22} = \sigma_y$  (kPa) in the concrete slab resting on the lean concrete substructure: friction coefficient  $\mu = 0.5$ ,  $k_z = 10,000$  kN/m<sup>3</sup>.

Table 3: Stresses  $S_{11} = \sigma_x$  and  $S_{22} = \sigma_y$  depending on stiffness  $k_z$  and friction coefficient  $\mu$ .

Numerical model	$\mu$ (-)	$k_z$ (kN/m <sup>3</sup> )	$S_{11} = \sigma_x$ (MPa)		$S_{22} = \sigma_y$ (MPa)	
			Max.	Min.	Max.	Min.
Model 'A'	0.08	50,000	0.4198	-0.0199	0.1949	0.0228
Model 'A'	0.1	50,000	0.5191	-0.0245	0.2427	0.0282
Model 'B'	0.1	10,000	4.7610	0.2423	3.1130	0.2116
Model 'B'	0.5	10,000	7.1070	0.3046	6.0280	0.3023
Model 'B'	0.1	50,000	4.9770	0.3585	3.4520	0.3234
Model 'B'	0.5	50,000	7.2040	0.5170	6.5430	0.5246
Model 'B'	0.1	100,000	5.0230	0.4017	3.5220	0.3636
Model 'B'	0.5	100,000	7.2210	0.6327	6.6160	0.6270

Table 4: Maximum stresses  $S_{11} = \sigma_x$  and  $S_{22} = \sigma_y$  depending on stiffness  $k_z$  and friction coefficient  $\mu$ .

$k_z$ (kN/m <sup>3</sup> )	$\sigma_x$ (MPa)	$\sigma_y$ (MPa)
$\mu$ (-)	0.1	0.5
10,000	4.761	3.113
50,000	4.977	3.452
100,000	5.023	3.522

Table 5: Change of maximum stresses  $\Delta\sigma_x$  and  $\Delta\sigma_y$  in relation to stresses for  $k_z = 10,000$  kN/m<sup>3</sup>.

$k_z$ (kN/m <sup>3</sup> )	$\Delta\sigma_x$ (%)	$\Delta\sigma_y$ (%)
$\mu$ (-)	0.1	0.5
10,000	0.0%	0.0%
50,000	4.5%	10.9%
100,000	5.5%	13.1%

Table 6: Change of maximum stresses  $\Delta\sigma_x$  and  $\Delta\sigma_y$  in relation to stresses for  $\mu = 0.1$ .

$k_z$ (kN/m <sup>3</sup> )	$\Delta\sigma_x$ (%)	$\Delta\sigma_y$ (%)
$\mu$ (-)	0.1	0.5
10,000	0.0%	49.3%
50,000	0.0%	44.7%
100,000	0.0%	43.8%

the substrate. This discrepancy could be attributed to the fact that model 'A' is a considerably more simplified model, that is, the friction between the mat foundation and the subsoil is modelled by reducing the stiffness values of the horizontal elastic bonds. These results serve to confirm the assumption that was made at the beginning of section 3, that is, that model 'A' underestimates the stresses in the concrete, and that model 'B' is a more appropriate model.

As shown in Table 4 and Figure 13, the maximum tensile stresses  $S_{11} = \sigma_x$  and  $S_{22} = \sigma_y$  are contingent on the stiffness  $k_z$  and the friction coefficient  $\mu$ . Table 5 and Figure 14 illustrate the variation in maximum stresses, designated as  $\Delta\sigma_x$  and  $\Delta\sigma_y$ , in relation to the stresses at  $k_z = 10,000$  kN/m<sup>3</sup>. The percentage change in stress was calculated using the following formula, for example:  $\Delta\sigma_x = (4.977/4.761 - 1) \times 100\% = 4.5\%$ . For a constant value of the friction coefficient  $\mu$ , increasing the value of stiffness coefficient  $k_z$  causes an increase in stresses  $\sigma_x$  and  $\sigma_y$  (see Table 4 and Fig. 13).

As shown in Table 6 and Figure 15, the percentage changes in maximum stresses, designated as  $\Delta\sigma_x$  and  $\Delta\sigma_y$ , are shown as a function of stresses for  $\mu = 0.1$ . In this instance, the percentage change in stress was determined using the following formula, for example:  $\Delta\sigma_x = (7.107/4.761 - 1) \times 100\% = 49.3\%$ . For a constant value of the stiffness coefficient  $k_z$ , an increase in the value of the friction

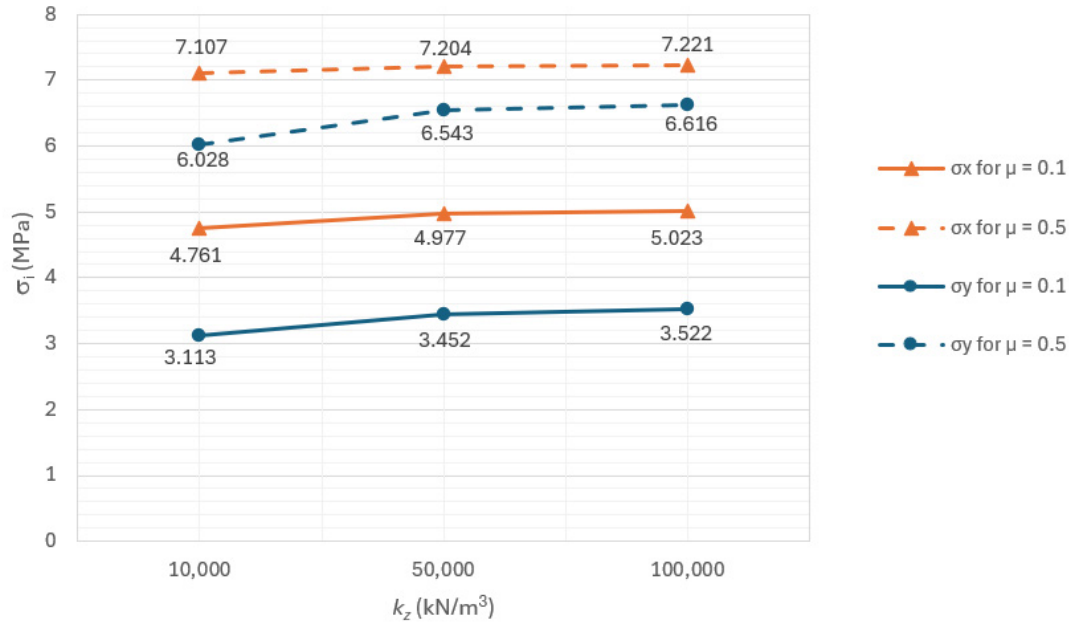


Figure 13: Maximum stress  $\sigma_x = S_{11}$  and  $\sigma_y = S_{22}$  depending on stiffness  $k_z$  and friction coefficient  $\mu$ .

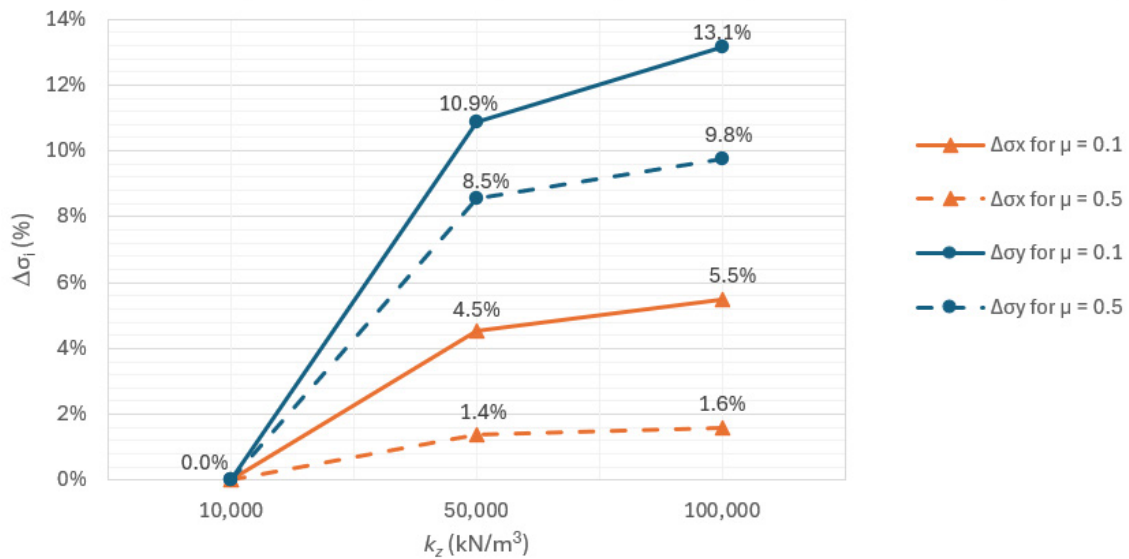


Figure 14: Change of maximum stresses  $\Delta\sigma_x$  and  $\Delta\sigma_y$  in relation to stresses for  $k_z = 10,000$  kN/m<sup>3</sup>.

coefficient  $\mu$  leads to an increase in stresses  $\sigma_x$  and  $\sigma_y$  (see Table 4 and Fig. 13).

As shown in Figure 15, an increase in the friction coefficient results in an increase in stress in the concrete. A five-fold increase in the friction coefficient, and thus a five-fold increase in the friction forces, results in an average increase of less than one and a half times the stress in the concrete (146% to be precise) in the  $x$ -direction, the contact pressure of which remains unchanged. Conversely,

the  $y$ -direction shows a more substantial increase, with a similar alteration in the friction coefficient yielding an average increase of less than a factor of two in stress (an increase of 190%, to be precise).

As shown in Figures 16 and 17, it can be concluded that the influence of sub-base stiffness is significant in the case of weak soils; for soils defined as medium or strong ( $k_z = 50,000$  kN/m<sup>3</sup> or  $k_z = 100,000$  kN/m<sup>3</sup>), no significant change in results is observed.

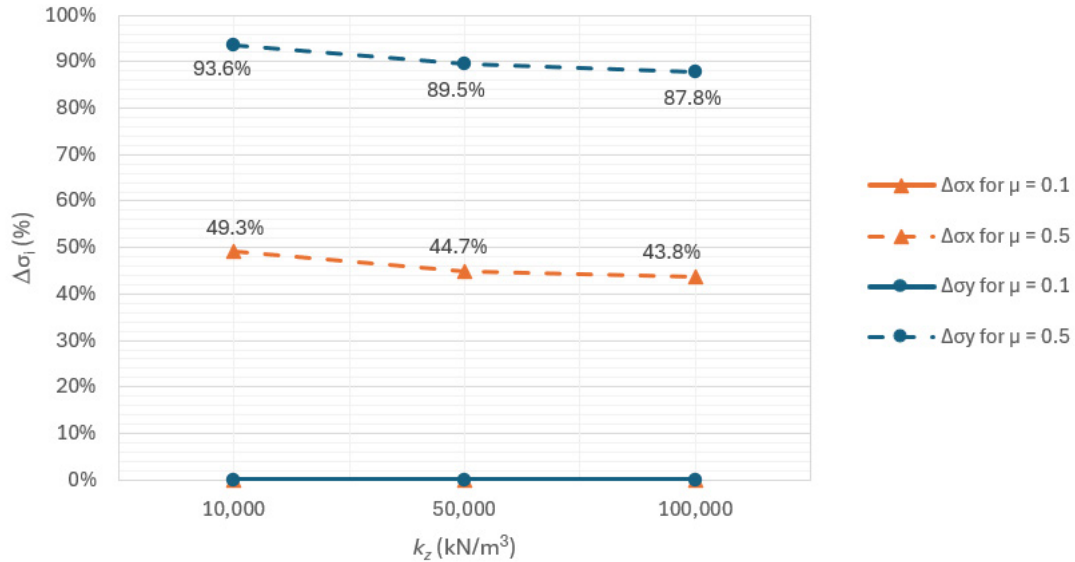


Figure 15: Change of maximum stresses  $\Delta\sigma_x$  and  $\Delta\sigma_y$  in relation to stresses for  $\mu = 0.1$ .

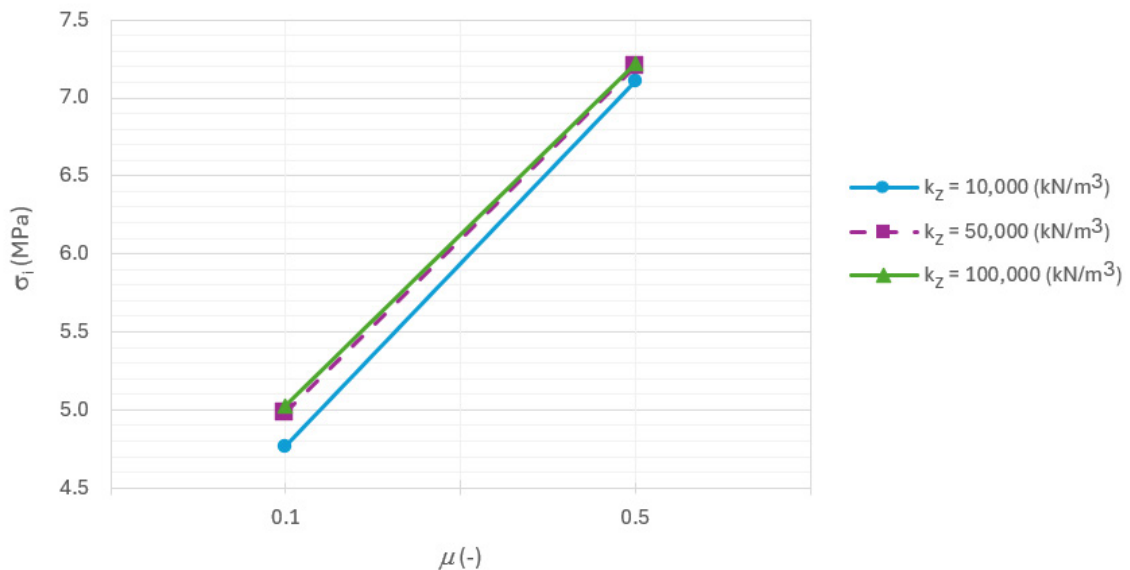


Figure 16: Maximum stress  $\sigma_x$  depending on the friction coefficient  $\mu$  and stiffness  $k_z$ .

## 4 Conclusions and summary

The numerical analyses conducted in this study indicate that the conventional method of modelling the interaction of the structure with the soil, namely the Winkler basis, does not adequately account for the shrinkage stresses in reinforced concrete elements. It is, therefore, recommended that this connection be modelled with greater precision than the linear-elastic Winkler model, for instance, by employing the interaction model of the Mohr-Coulomb

substrate, which has been analysed in this paper. This conclusion is significant, given that the Winkler model is predominantly employed in design practice. This model is accurate for calculating bending moments in slabs but is inadequate for evaluating shrinkage effects.

The significant discrepancies, observed in the results of models 'A' and 'B' (rows 2 and 3 of Table 3), with an 11-fold increase in  $\sigma_x$  stresses and a 15-fold increase in  $\sigma_y$  stresses in model 'B', confirm that the Winkler model is insufficient to adequately model the shrinkage of concrete

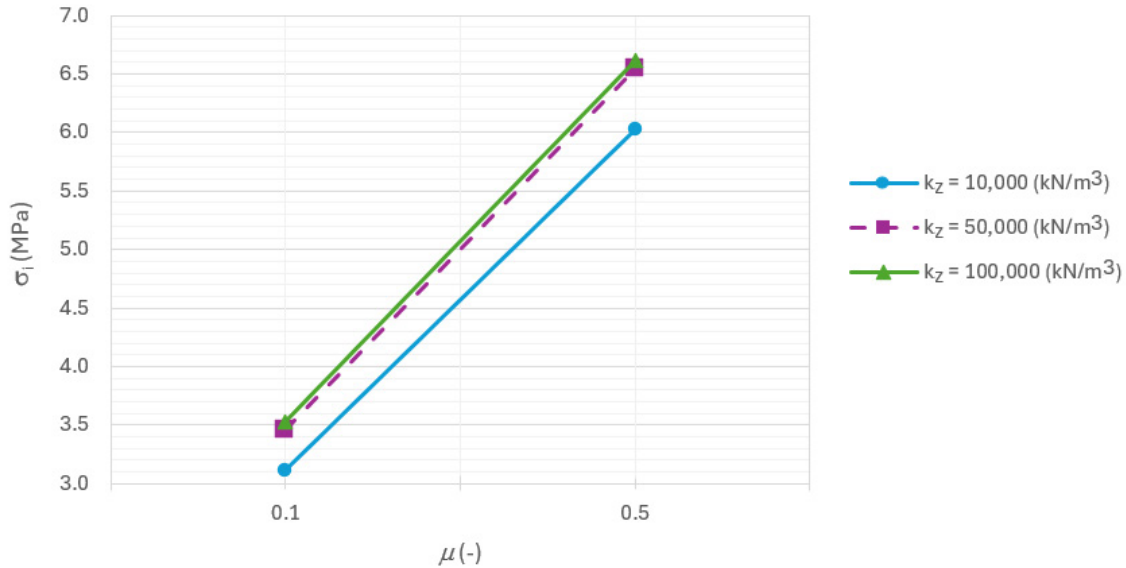


Figure 17: Maximum stress  $\sigma_y$  depending on the friction coefficient  $\mu$  and stiffness  $k_z$ .

elements under substrate interaction conditions. These differences, exceeding an order of magnitude, underscore the limitations of the Winkler’s model.

The next research step, already mentioned in this article, is to investigate the influence of foundation loading and the consequent increase in frictional forces between the foundation and the subsoil, while considering the influence of shrinkage from drying. In future research, it would be worthwhile to carry out a numerical analysis of the shrinkage of mat foundations and footings founded on cohesive and non-cohesive soils. Further analyses should also consider a certain series of footing types, that is, the most typical dimensions of the structure and, more specifically, the aspect ratio, degree of reinforcement and soil types.

## References

- [1] Gilbert, R.I., Ranzi, G. (2011). *Time-Dependent Behaviour of Concrete Structures*. Spon Press, London and New York.
- [2] Džolan, A., Kožul, M., Harapin, A., Čubela, D. (2020). Analysis of the concrete shrinkage effects on the real behavior of the spatial concrete and reinforced concrete structures using the thermal analogy. *Engineering Computations*, 37(4), 1451-1472.
- [3] Gribniak, V., Kaklauskas, G., Bacinskas, D. (2008). Shrinkage in reinforced concrete structures: a computational aspect. *Journal of Civil Engineering and Management*, 14(1), 49–60.
- [4] Neville, A. M. (2011). *Properties of concrete*. Pearson, London.
- [5] Gribniak, V., Kaklauskas, G., Kliukas, R., Jakubovskis, R. (2013). Shrinkage effect on short-term deformation behavior of reinforced concrete – When it should not be neglected. *Materials and Design*, 51, 1060–1070.
- [6] Bažant, Z.P. (1975). Theory of creep and shrinkage in concrete structures: a precise of recent developments. *Mechanics Today*, 2, edited by Nemat-Nasser, S., Pergamon Press, New York, USA.
- [7] Dacko, M., Nowak, J. (2010). Numerical simulation of stress and strain state induced by shrinkage of concrete in large-size plate. *Journal of KONES Powertrain and Transport*, 17(1), 93-99.
- [8] Flaga, K. (2002). *Shrinkage of concrete and its effect on load-bearing capacity, serviceability and durability of reinforced and prestressed concrete structure*. Wyd. PK. Kraków. [in Polish].
- [9] Shadravan, S., Ramseyer, Ch., Kang, T. H.-K. (2015). A long term restrained shrinkage study of concrete slabs on ground. *Engineering Structures*, 102, 258-265. <https://doi.org/10.1016/j.engstruct.2015.08.018>.
- [10] Golubińska, A., Grzeszykowski, B., Knauff, M. (2018). *Calculation examples for reinforced concrete structures*. Volume 3, Crackig, Wydawnictwo Naukowe PWN. Warszawa. [in Polish]
- [11] Flaga, F., Furtak, K., Jargiełło, J. (1984). Application of the modified ageing theory to the estimation of compressive stress relaxation in reinforced concrete elements, *Archiwum Inżynierii Lądowej*, XXX (4), PWN. 665-676. [in Polish]
- [12] *Abaqus FEA software*, Dassault Systemes, <https://academy.3ds.com>.
- [13] Bowles, J. (1996). *Foundation Analysis and Design*. McGraw Hill.
- [14] Klemczak, B., Flaga, K., Knoppik-Wróbel, A. (2017). Analytical model for evaluation of thermal–shrinkage strains and stresses in RC wall-on-slab structures, *Archives of Civil and Mechanical Engineering*, 17(1), 75-95.
- [15] Eurocode 2 - Design of concrete structures - Part 1-1: General rules and rules for buildings, bridges and civil engineering structures EN 1992-1-1: 2024-05.
- [16] [http://www.leschuplast-glt.de/sitemap\\_gleitlagertechnik\\_en.html](http://www.leschuplast-glt.de/sitemap_gleitlagertechnik_en.html), access: 02.2025.